

Turbulent transport measurements for a GT mixing device

Gobyzov O.A.¹, Dulin V.M.^{1,2}, Chikishev L.M.^{1,2}, Lobasov A.S.^{1,2}, Sharaborin D.K.^{1,2}, Bilsky A.V.^{1,2}, Tsatiashvili V.V.³, Avgustinovich V.G.³, Markovich D.M.^{1,2}

¹Institute of Thermophysics SB RAS, Novosibirsk, Russia

²Novosibirsk State University, Novosibirsk, Russia

³JSC «Aviadvigatel», Perm, Russia

*corresponding author: oleg.a.g.post@gmail.com

Abstract Present paper reports an evaluation and interpretation of the data, acquired from PIV/PLIF experiment performed in a model of combustion chamber with an industrial mixing device, developed by JSC «Aviadvigatel». Experiments were carried out in a non-reacting flow at overpressure conditions. Separate and simultaneous PIV/PLIF measurements were carried out, and a set of image and data correction procedures were performed in order to minimize uncertainty due to imperfect optical access and limited spatial resolution. An image pre-processing was performed to reduce an artificial “stripes” introduced by inhomogeneous lighting. Effect of spatial resolution on velocity, velocity gradient, and turbulent kinetic energy (TKE) were analyzed. On the basis of PIV measurements, approximate TKE dissipation rate was evaluated by means of LES-based correction model. Turbulent mass flux over the measurement area was retrieved from simultaneous PIV/PLIF data and an analysis of the gradient closure hypothesis was performed.

Keywords: PIV, PLIF, turbulent transport, GT mixing device.

Introduction

Numerical codes for turbulent mixing calculations for GT burners require verification by comprehensive experimental data, which is often a challenging task to provide. Conventional single-point measurements usually have high temporal resolution but do not provide information about spatial features of the flow and turbulent transport. Contrary to that, planar optical methods, like PIV and PLIF can take advantage of capturing the instantaneous distributions of flow velocity and passive admixture concentration. Such data are usually more adequate for numerical code verification.

Raw experimental data retrieved from PIV and LIF measurements can undergo certain distortions due to experimental conditions or limitations of the measurement technique. Proper evaluation of such data is always a challenging task, but, if performed, can provide more complex analysis and validation of CFD codes. In the paper different steps in PIV/PLIF data evaluation are considered for the series of experiments, performed in high Reynolds number flow ($Re \approx 10^5$) in GT combustion chamber model. There is quite limited number of simultaneous PIV/PLIF investigations published so far. One of such works was carried out earlier by Heinze et. al. [1] in a small scale wind tunnel in DLR. In this work authors performed acetone-based PLIF/PIV experiments to retrieve turbulent mass flux from the experimental data. The work was focused mainly on experimental technique and analysis of error sources. High-speed stereo-PIV/LIF-OH data were presented by Boxx et. al. in [2]. Taking advantage of high speed simultaneous velocity and temperature measurements authors performed a comprehensive analysis of the reacting flow in DLR Dual-Swirl Gas Turbine Model Combustor. Authors have detected presence of OH pockets and described their development in time, analyzed vortex-flame interaction dynamics and revealed spatial POD-eigenmodes in the flow. Current paper, in contrast to those mentioned above, is focused on the assessment and evaluation of the raw low-repetition experimental data for turbulent mass transport and turbulent statistics investigations rather than on the experimental technique.

Experimental setup and equipment

Experiments were carried out in GT combustion chamber model. Model consisted of plenum chamber with mixing device installed inside of it and a test section. Test section, starting immediately after the mixing device, was bounded by quartz cylinder (inner diameter 120 mm, see fig. 1). Diameter of the mixing device exit d was 80 mm.

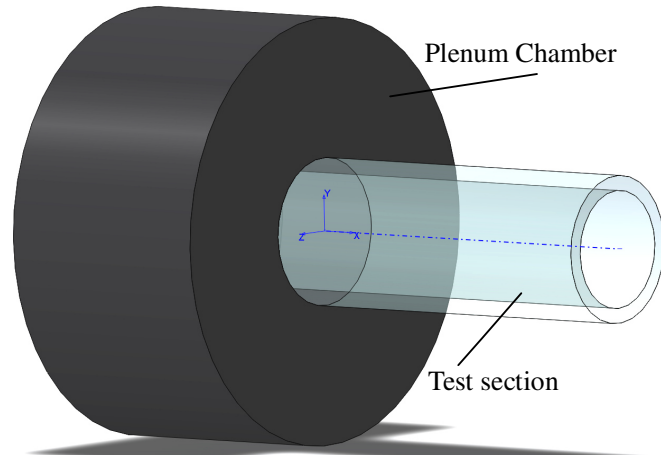


Fig. 1 Test section of the GT combustion chamber model

Planar PIV experiments were performed in YZ plane at the distance of $0.1 \cdot d$ and $1 \cdot d$ from the mixing device exit and in XY plane immediately after the mixing device. Water-glycerol tracer particles generated by Laskin-nozzle based seeding device were introduced into the flow. Admixture concentration measurements (PLIF) were implemented with the acetone injected as a vapor into the flow following [3] and [4]. Acetone was admixed to the neon gas which was used as a model gas for the fuel mixture.

Simultaneous PIV/PLIF measurements were also performed in XY plane immediately after the mixing device, and reconstruction procedure based on the image of calibration target was applied to align PIV and PLIF images in space.

Image quality and correction procedures

Due to inclusions in side surface of the cylinder laser sheet used for PIV also had large number of stripy inhomogeneities. It resulted in distorted data retrieved from PIV evaluation: stripy structure emerged in average velocity fields, and especially in higher order moments. An approach similar to light sheet correction in PLIF was adapted to correct an intensity of particle images.

To reduce this effect intensity of each image was filtered in the following way: since the inhomogeneities were produced by stationary defects in the cylinder material, intensity of each pixel was corrected by the time-averaged intensity:

$$I^*(X, Y) = \frac{I(X, Y)}{\langle I(X, Y) \rangle} I_0 \quad (1)$$

where I_0 is the mean of the time-averaged intensity:

$$I_0 = \frac{1}{n} \sum_x \sum_y \langle I(X, Y) \rangle \quad (2)$$

This procedure, although not fully compensating lighting flaws, substantially improved quality of particle images and reduced impact of “stripes” on velocity fields. Average velocity components, shown in fig.2 have proved that in general flow has an axisymmetric structure, albeit some skewness can be observed.

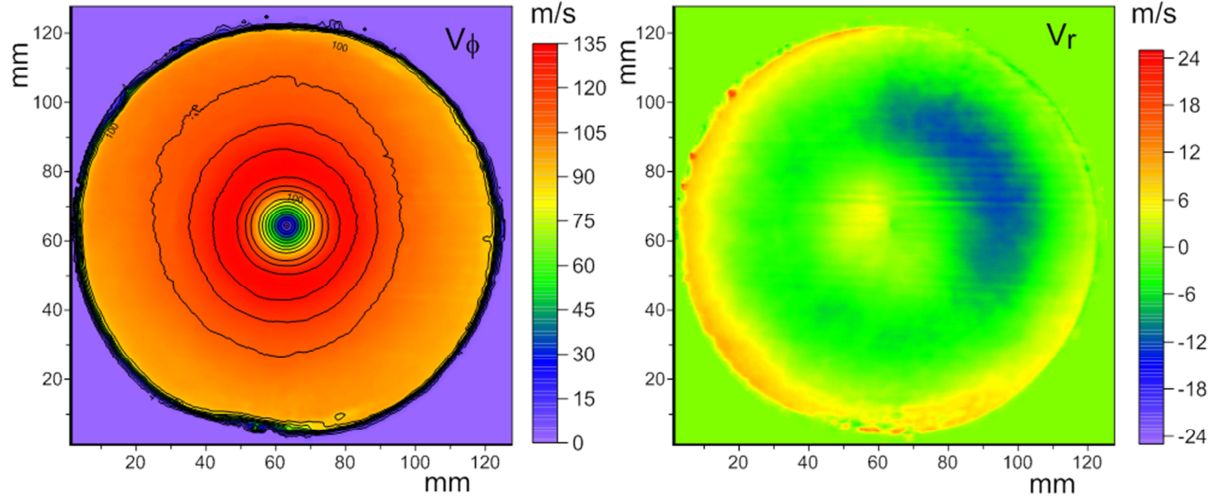


Fig. 2 Average velocity components distribution in YZ plane at the distance of 1d from mixing device exit.

PIV interrogation scheme

Velocity data was retrieved from images using PIV cross-correlation algorithm with 75% interrogation window overlap. Interrogation was performed in 4 iterations, with one grid refinement after the second iteration. Velocity data was filtered using range validation filter and signal-to-noise filter. In turbulent statistics false vectors were just excluded from evaluation, but for the calculation of spatial derivatives additional adaptive median filtering and moving average interpolation of false vectors was applied to form a datasets on a regular grid.

Spatial resolution, as reported in [5, 6], and many other works, can have a substantial impact on the results of investigation. Apparently, PIV experiment in high-Reynolds number flow usually unable to fetch turbulent features at small scales, but the higher spatial resolution is, the larger part of the turbulent spectra would be resolved. One should also take into account that PIV resolution is bounded above due to spatial averaging over the light sheet thickness. In the present experiments light sheet thickness (≈ 1 mm) didn't exceed the size of interrogation window. There are two ways to vary a spatial resolution in PIV experiment: variation of optical magnification factor and the size of interrogation window in PIV algorithm. In the experiments under consideration it was important to perform measurements across the whole test section, and therefore optical magnification was selected to satisfy this condition and was fixed during the series of experiments. As for the variation of interrogation window, excessive reduction of its size can result in emergence of intense data noise. If higher order statistical moments or spatial derivatives are to be retrieved from PIV velocity fields, than noise amplification due to numerical calculation of derivatives should be taken into account.

To assess an effect of spatial resolution Δ , or rather of the interrogation window size, velocity field calculation was performed with final window size varied from 16×16 pix. to 128×128 pix. (see fig.3). Even with qualitative analysis, it can be concluded that 16×16 pix. window interrogation introduces large amount of high-frequency noise, which contributes into the measured TKE component, and if smoothed, distorts the profile in the area of low velocity pulsations. In its turn 128×128 pix. window interrogation results in substantial underestimation of TKE component, especially in the mixing layer. For 32×32 pix. and 64×64 pix. window almost no high-frequency noise component is observed, but larger interrogation window predictably yields a bit lower intensity of velocity pulsations. Same arguments can be applied to the second-order of velocity derivatives. In the final analysis an interrogation scheme with window size of 32×32 pix. was chosen for further evaluation. Since, in all cases spatial overlap rate between the interrogation areas was 75% the grid step h was four times smaller than Δ .

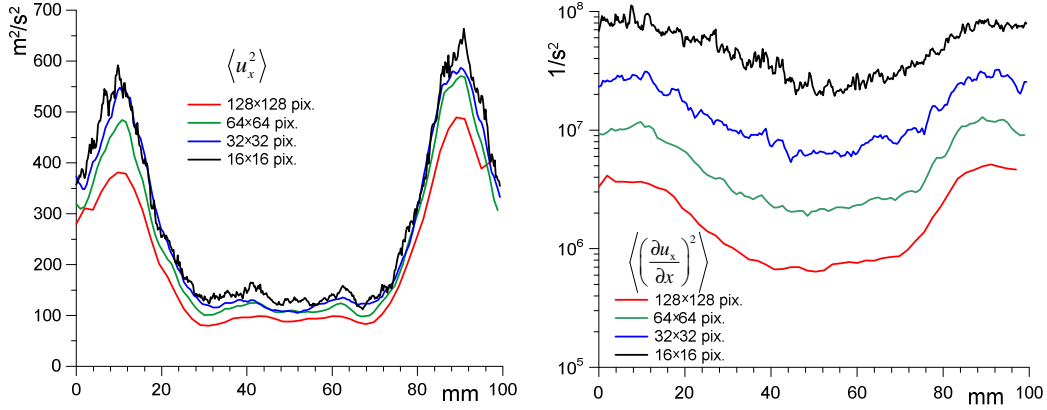


Fig. 4 TKE component and second-order of velocity derivative profiles along Y axis at the distance of 22 mm from the mixing device exit.

Turbulent kinetic energy dissipation rate

A turbulent kinetic energy (TKE) dissipation rate per unit volume depends on local kinematic viscosity of the fluid and strain rate tensor S_{ij} :

$$S_{ij} = \frac{1}{2} \left(\frac{\partial u_i}{\partial x_j} + \frac{\partial u_j}{\partial x_i} \right) \quad (3)$$

And TKE dissipation rate is:

$$\varepsilon = 2\nu \langle S_{ij} S_{ij} \rangle \quad (4)$$

Expressed in simple algebraic form, equation (4) will contain 12 second order-moments of velocity derivatives. Thus, in order to obtain TKE dissipation rate directly from the experiment, all 3 components of velocity vector should be measured, and measurement spatial resolution should be sufficient to resolve finest spatial scales in the flow without introducing truncation error in spatial derivatives calculation. Usually such experimental data is unavailable, especially for high-Reynolds number flows: velocity data may be incomplete, contain noise and lack spatial resolution. In some cases, proper physical assumptions can be applied to reduce number of velocity components needed to estimate TKE dissipation rate. Besides, numerical differentiation scheme should be carefully chosen in order to keep proper balance between measurement noise amplification and truncation error.

For the case under consideration several numerical differential schemes were considered for calculation of spatial velocity derivatives (see. Fig 5). Among these schemes were: simple central differentiation (eq. 5), least-squares (eq. 6) scheme with different point spacing H , proposed in [7], and Richardson extrapolation scheme optimized for minimization of random error amplification (eq.7).

$$\frac{\partial u(x)}{\partial x} = \frac{u(x+H) - u(x-H)}{2H} \quad (5)$$

$$\frac{\partial u(x)}{\partial x} = \frac{2u(x+2H) + u(x+H) - u(x-H) - 2u(x-2H)}{10H} \quad (6)$$

$$\frac{\partial u(x)}{\partial x} = \frac{16u(x+4H) + u(x+H) - u(x-H) - 16u(x-4H)}{130H} \quad (7)$$

Profile of the second-order velocity derivative in a transversal cross-section of the measurement area at the distance of $1d$ from burner exit evaluated with different numerical derivation schemes is shown in fig.5. It can be seen, that simple central differentiation scheme and least-squares with $H=h$ introduce amount of noise comparable to the signal amplitude, while for least-square scheme with $H \geq 2h$ amount of high-frequency noise doesn't differ much, but truncation error increases significantly with increase of H . Note that least-square with $H=2h$ and Richardson scheme with $H=1h$ yield almost similar results because terms $u(x \pm 4h)$ contribute most in both cases. According to this results, least-squares differential scheme with $H=2h$

was chosen for further evaluation.

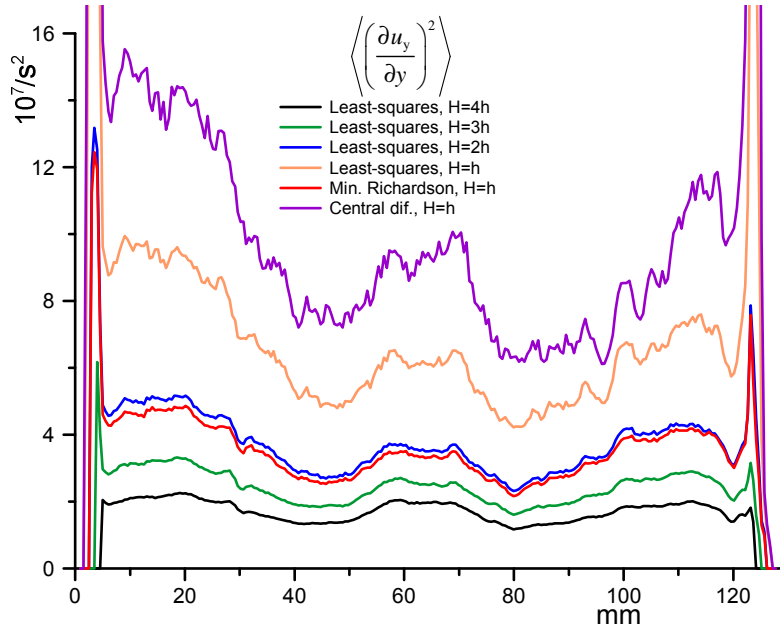


Fig. 5 Second-order velocity derivative profile along Z axis at the distance of 1d from the mixing device exit evaluated with different numerical derivation schemes

As PIV experimental data contained only two velocity components in XY plane, direct TKE dissipation rate calculation from eq.4 wasn't possible. At the same time, according to the statistical data yielded from measurements taken in YZ plane, an assumption of rotational symmetry about X axis was quite appropriate despite of some skewness. Under this assumption formulation proposed by Hussain et. al. in [8] for TKE dissipation rate calculation can be applied. In this formulation only four second order-moments of velocity derivatives are used:

$$\varepsilon = \nu \left[-\left\langle \left(\frac{\partial u_1}{\partial x_1} \right)^2 \right\rangle + 2 \left\langle \left(\frac{\partial u_1}{\partial x_2} \right)^2 \right\rangle + 2 \left\langle \left(\frac{\partial u_2}{\partial x_1} \right)^2 \right\rangle + 8 \left\langle \left(\frac{\partial u_2}{\partial x_2} \right)^2 \right\rangle \right] \quad (8)$$

Eventually, if velocity derivatives calculated from experimental data using least-square scheme is substituted in eq. (5), ε yielded from this equation, here and below addressed as ε^m , will qualitatively represent distribution of TKE dissipation rate, but quantitatively will greatly underestimate the value. The latter statement can be indirectly confirmed by the following considerations: coarse estimation of Kolmogorov's scale η as $Re^{-3/4}$ yields $\eta \approx 50 \mu m$, while PIV spatial resolution, taking into account interrogation window overlap, was ≈ 1.5 mm, and additional spatial filtering was introduced by numerical differentiation scheme. Consequently, for such measurement data large part of the spectrum falls into sub-grid scale, and, therefore, missed in TKE dissipation rate estimation.

To assess an «underestimation factor» a «LES-fundamental» approach [9] together with appropriate model of turbulence can be applied. In this approach turbulence is assumed to conform to the selected model and limited spatial resolution of the measurement technique considered as a low-pass filter. Though PIV spatial filter is, in general, considered to behave like a cardinal sine function [10], for simplicity here it will be considered a sharp cut-off filter with $k_{max} = \pi/\Delta$, where spatial resolution is homogeneous in x and y directions $\Delta = \Delta_x = \Delta_y$. For the case, Δ was equal to $8h$, where h is a step between velocity vectors in a PIV velocity field. Factor 8 for the Δ was chosen because of 75% window overlap in PIV interrogation and decrease in effective spatial resolution for velocity derivatives due to selected numerical differentiation scheme.

The Smagorinsky model for turbulent viscosity ν_τ is:

$$\nu_\tau = C_s^2 \Delta^2 \sqrt{\left(2S_{ij}^* S_{ij}^* \right)} \quad (9)$$

Where S_{ij} is strain rate tensor, Δ is the filter width, C_s is the Smagorinsky coefficient, and symbol * indicates

instantaneous quantity. According to [11] and some other works ensemble averaging operator can be introduced on the norm of the strain-rate tensor without loss of the models performance:

$$v_\tau \approx C_s^2 \Delta^2 \left\langle 2\overline{S_{ij}^* S_{ij}^*} \right\rangle^{1/2} \approx C_s^2 \Delta^2 \left\langle 2\overline{S_{ij} S_{ij}} \right\rangle^{1/2} \quad (10)$$

Under the assumption of infinite Re TKE dissipation rate can be expressed from eq. 4 as

$$\varepsilon \approx 2v_\tau \left\langle \overline{S_{ij}^* S_{ij}^*} \right\rangle \approx 2v_\tau \left\langle \overline{S_{ij} S_{ij}} \right\rangle \quad (11)$$

For the inertial range spectrum, filtered by a sharp cut-off filter with width= Δ the value of C_s can be obtained as:

$$C_s = \frac{1}{\pi} \left(\frac{2}{3C} \right)^{3/4} \approx 0.173, \quad (12)$$

Where $C \approx 1.5$ is Kolmogorov constant. In [12] other approximations, including an approximation for the case $L/\Delta \gg 1$ (13) were proposed:

$$\varepsilon = 2v_\tau \left\langle \overline{S_{ij}^* S_{ij}^*} \right\rangle, \text{ where } v_\tau = \sqrt{(C_{s,\infty} \Delta / \gamma)^4 \left(2\overline{S_{ij}^* S_{ij}^*} \right) + v^2} - v \quad (13)$$

In this case, turbulent kinetic energy dissipation is given as a sum of sub-grid-scale and resolved dissipation, and γ depends on the filter shape and is equal to a unit for a sharp cutoff filter.

Recalling that resolved scales in this analysis corresponds to that measured with PIV, a relation (14) with classical Smagorinsky or modified model for turbulent viscosity can be applied to correct data for the amount of TKE dissipation rate at not resolved scales:

$$\varepsilon = v_\tau \varepsilon^m / \nu, \text{ where } v_\tau = C_s^2 \Delta^2 (\varepsilon^m / \nu)^{1/2} \text{ or } v_\tau = \sqrt{(C_s \Delta / \gamma)^4 (\varepsilon^m / \nu) + \nu^2} - \nu \quad (14)$$

In accordance with the model described above a «correction factor» of the TKE dissipation rate over the measurement area was calculated and «corrected» TKE dissipation rate was assessed (fig.6). Predictably, an area of the maximum TKE dissipation rate corresponds to the region of most intense large-scale eddy interaction with the small-scale turbulence in the mixing layer. A «correction factor» exceeds 600 over the whole measurement area and in the mixing region goes as high as 10^3 .

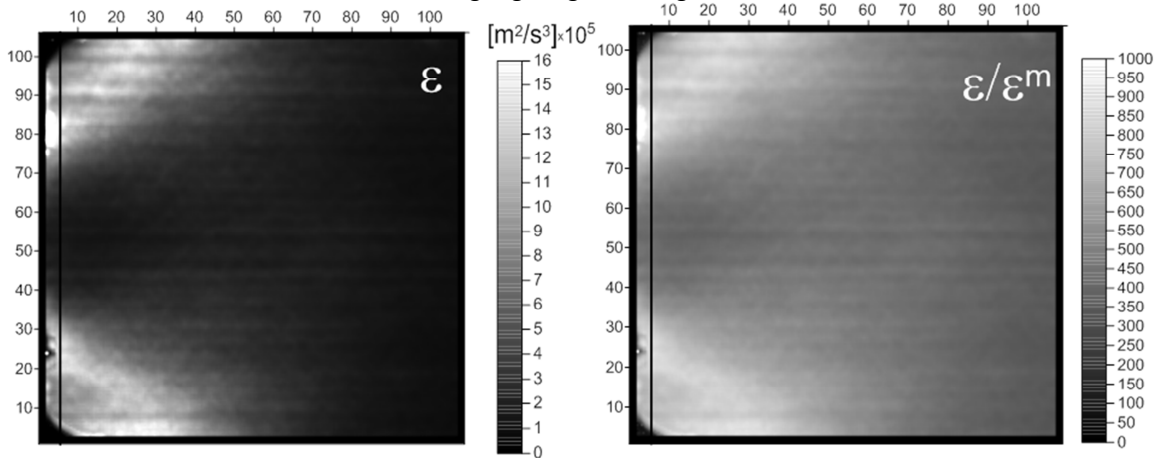


Fig. 6 Distribution of TKE dissipation rate and «correction factor» over the measurement area in XY plane

Turbulent passive species transport

A conservation equation of species for turbulent flows can be written as:

$$\frac{\partial \bar{c}}{\partial t} + \bar{u}_j \frac{\partial \bar{c}}{\partial x_j} = \frac{D \partial^2 \bar{c}}{\partial x_j^2} - \frac{\partial \langle u_j c \rangle}{\partial x_j} \quad (15)$$

where \bar{c} is the time-averaged concentration, c - the concentration fluctuation, \bar{u}_j - time averaged velocity component, u_j - fluctuation of velocity component, D - molecular diffusion coefficient.

Right-hand part of the equation represents mass transport. In high-Reynolds number turbulent flows molecular diffusion term $D\frac{\partial \bar{c}}{\partial x_j}$ is usually negligible comparing to the turbulent diffusion term $\langle u_j c \rangle$, and can be omitted [13]. Then conservation equation takes following form:

$$\frac{\partial \bar{c}}{\partial t} + \bar{u}_j \frac{\partial \bar{c}}{\partial x_j} = -\frac{\partial \langle u_j c \rangle}{\partial x_j} \quad (16)$$

For this equation in CFD models a closure problem is usually solved by the assumption that turbulent mass transport is proportional to the mean concentration gradient (Fick's diffusion law assumption).

$$\langle u_j c \rangle = Dt_j \frac{\partial \bar{c}}{\partial x_j} \quad (17)$$

Yet, to validate the model, fidelity of this assumption should be performed. For the experiments under consideration validation of Fick's law assumption was performed using PIV and PLIF experimental data. In fig. 7 a distribution of y -component of $\langle u_j c \rangle$ and y -component of the mean admixture concentration gradient are presented. An area of the reversed flow is bounded by the solid line in the figure. Using these two distributions a turbulent admixture diffusion Dt coefficient can be assessed.

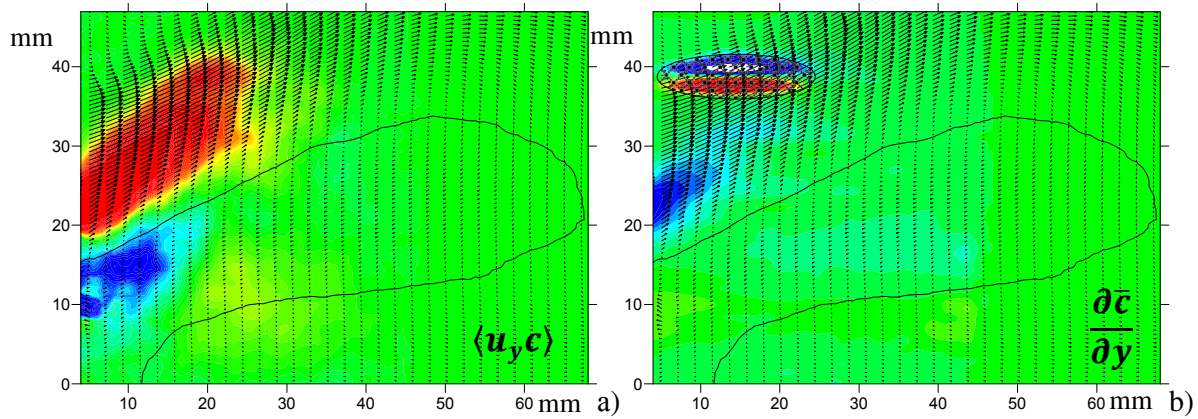


Fig. 7 y -component of $\langle u_j c \rangle$ and y -component of the mean admixture concentration gradient

In fig.8 a profile of y -component of $\langle u_j c \rangle$ and y -component of the mean admixture concentration gradient across the measurement area is shown. It can be seen from the figure that directly measured turbulent transport is in good correspondence with the Fick's diffusion law, though a small area of counter-gradient transport can be observed at $y \approx 10$ mm.

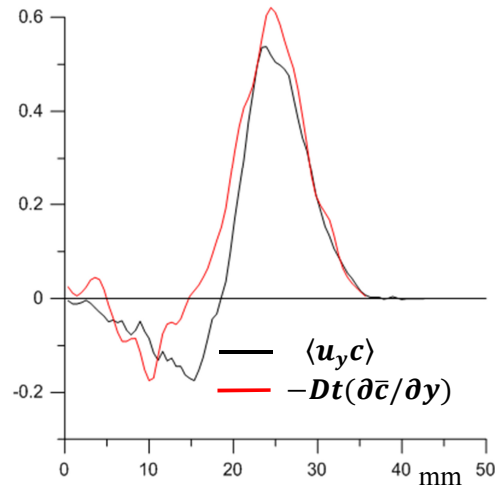


Fig. 8 profile of y-component of $\langle u_y c \rangle$ and y-component of the mean admixture concentration gradient across the measurement area

Another representative characteristic that can be recovered from simultaneous PIV/PLIF measurements is turbulent Schmidt number, which represents the ratio between the rates of turbulent transport of momentum and the turbulent mass transport.

As Schmidt number $Sc_t = \nu_t / Dt$, a distribution of ν_t is required to calculate Sc_t over the measurement area. Such distribution is available from PIV data through distribution of Reynolds stress and mean velocity gradient component, which are presented in fig. 9. As can be seen from the figure, maximum and minimum of both differ in sign and are reached within the shear layers of the swirling flow.

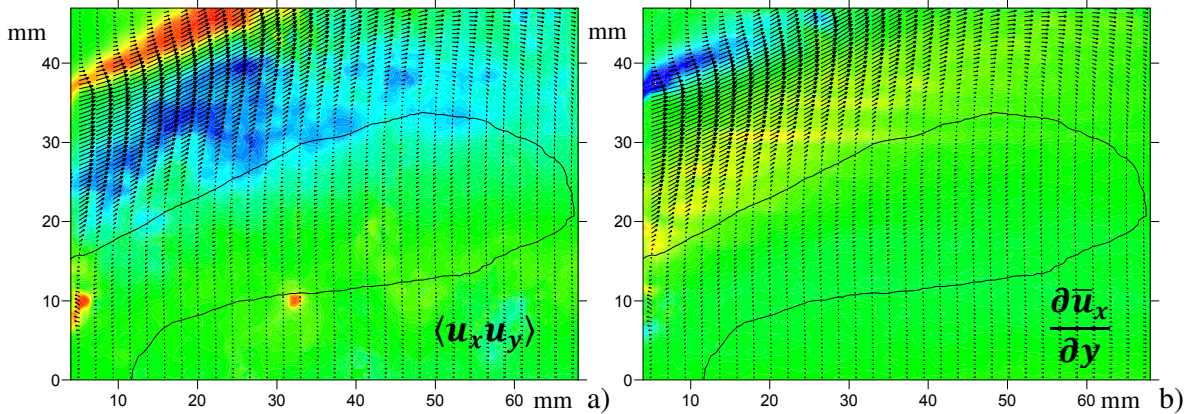


Fig. 9 distribution of Reynolds stress component and mean velocity gradient component

Conclusion

In the present work PIV/PLIF experimental data evaluation techniques for assessment of TKE dissipation rate and turbulent passive admixture transport in GT burner model were considered. TKE dissipation rate was calculated from 2D-PIV data using an assumption of rotational symmetry. «Correction factor» of the measured TKE dissipation rate was assessed through the «LES-fundamental» approach. Worth noting, that «Underestimation factor» appeared to be extremely large for the case, which is not surprising as Re was high ($\approx 3 \cdot 10^5$) and PIV spatial resolution was quite low. However, that means that only general features of the flow were fetched as the result of evaluation.

Turbulent passive admixture transport characteristics, namely turbulent diffusion coefficient and turbulent viscosity, required for application of gradient closure hypothesis and evaluation of turbulent Schmidt number were retrieved from the PIV/PLIF simultaneous measurements. It was also shown, that in general, Reynolds stresses and turbulent passive admixture flux, both conform to the gradient closure hypothesis.

Acknowledgments

This work was funded by a grant from the Russian Science Foundation (project No. 14-29-00203 in NSU, supervised by Professor Kemal Hanjalic).

References

- [1] Klinner J., Mayer V., Heinze J., Willert C. (2014) Simultaneous Measurements of Mixing Fraction and Velocities of a Coaxial Jet in a Turbulent Channel Flow, 17th International Symposium on Applications of Laser Techniques to Fluid Mechanics. 7-10 July 2014, Lisbon, Portugal, ISBN 978-989-98777-8-8.
- [2] Boxx I., Stöhr M., Carter C., Meier W., (2010) Temporally resolved planar measurements of transient phenomena in a partially pre-mixed swirl flame in a gas turbine model combustor, *Combustion and Flame*, vol. 157, pp. 1510 - 1525.
- [3] Bryant RA, Donbar JM, Driscoll JF (2000) Acetone laser induced fluorescence for low pressure/low temperature flow visualization. *Experiments in Fluids* 28(5) pp. 471–476
- [4] Lozano A., Yip B., Hanson R. (1992) Acetone: a tracer for concentration measurements in gaseous flows by planar laserinduced fluorescence. *Experiments in Fluids* 13 (6), pp. 369–376.
- [5] Alekseenko S., Bilsky A., Dulin V., Ilyushin B., Markovich D. (2005) Non-intrusive determination of turbulent energy balance in free and confined jet flows. // Proc. 4th International Symposium on Turbulence and Shear Flow Phenomena, Williamsburg, VA, USA, 27-29 June
- [6] Foucaut J.M, Milliat B., Perenne N., Stanislas M. (2004) Characterization of different PIV algorithms using the EUROPIV Synthetic Image Generator and real images from a turbulent boundary layer // Proc. EUROPIV 2 Workshop on Particle Image Velocimetry, Springer, Berlin. pp. 163–86.
- [7] Raffel M., Willert C., Wereley S., Kompenhans J. (2007) Particle Image Velocimetry. A practical guide, Second Edition, Berlin, Springer.
- [8] George W.K., Hussein H.J. (1991) Locally axisymmetric turbulence. // *J. Fluid Mech.*, Vol. 233, pp. 1-23
- [9] Dulin V.M., Marlovich D.M., Alekseenko S.V. Stereo PIV measurements of fine-scale turbulence statistics in a free jet flow ...
- [10] Foucaut J.M., Carlier J., Stanislas M. (2004) PIV optimization for the study of turbulent flow using spectral analysis. *Meas Sci Technol* Vol.15, pp. 1046-1058.
- [11] McMillan O. J., Ferziger J. H. (1979) Direct testing of subgrid-scale models. *AIAA J.* 17, pp. 1340–1346.
- [12] Meyers J., Sagaut P. (2006) On the model coefficients for the standard and the variational multi-scale Smagorinsky model. *J. Fluid Mech.*, vol. 569, pp. 287-319.
- [13] Roberts, P. J. W. and Webster, D. R., (2002), Turbulent diffusion, In: *Environmental Fluid Mechanics Theories and Application*, pp. 7-45, ASCE publications, Virginia.